Supplementary file

A multi-field coupling model for CO_2 enhanced shale gas recovery integrating chemical dissolution and mechanical weakening effects

Kang Yang[1], Yaobai Sun[1], Junping Zhou[2*], Qiao Chen[1], Guangrong Deng[3], Dasong Li[4]

[1]*Chongqing Institute of Green and Intelligent Technology, Chinese Academy of Sciences, Chongqing 400714, P. R. China*

[2]*State Key Laboratory of Coal Mine Disaster Dynamics and Control, Chongqing University, Chongqing 400044, P. R. China*

[3]*Department of Mechanical Engineering, Hong Kong Polytechnic University, Hong Kong 999077, P. R. China*

[4]*Chongqing River Affairs Center, Chongqing 401147, P. R. China*

E-mail address: yangkang@cigit.ac.cn (K. Yang); sunyaobai23@mails.ucas.ac.cn (Y. Sun); zhoujp1982@cqu.edu.cn (J. Zhou); chenqiao@cigit.ac.cn (Q. Chen); guangrong.deng@connect.polyu.hk (G. Deng); lidasongzz@163.com (D. Li).

[*]Corresponding author (ORCID: 0000-0002-7218-3235 (J. Zhou))

Yang, K., Sun, Y., Zhou, J., Chen, Q., Deng, G., Li, D. A multi-field coupling model for CO_2 enhanced shale gas recovery integrating chemical dissolution and mechanical weakening effects. Advances in Geo-Energy Research, 2025, 18(2): 180-194.

The link to this file is: https://doi.org/10.46690/ager.2025.11.07

Appendix A: Supplementary figures and tables

1. List of figures

2. List of tables

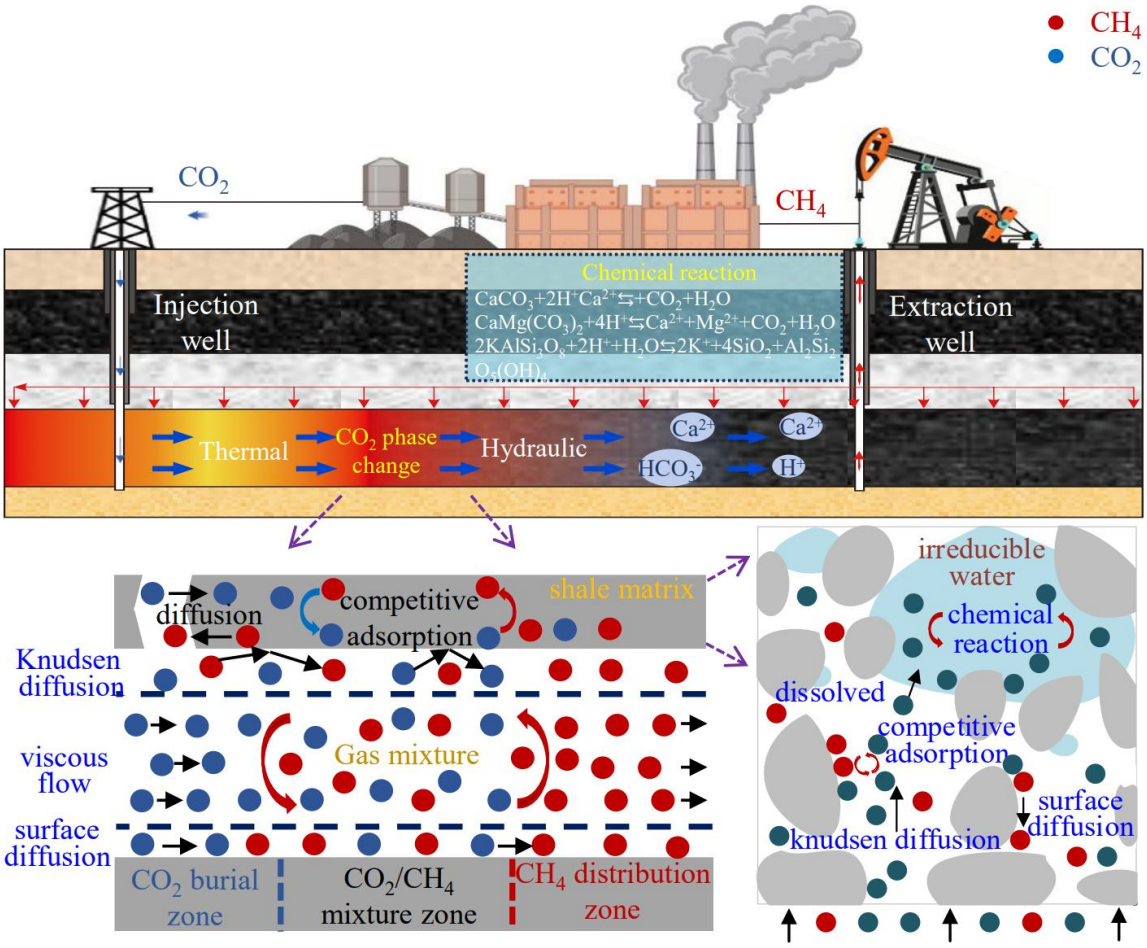

Fig.S1. Multi-field coupling mechanism in the reservoir during CO_2-ESGR.

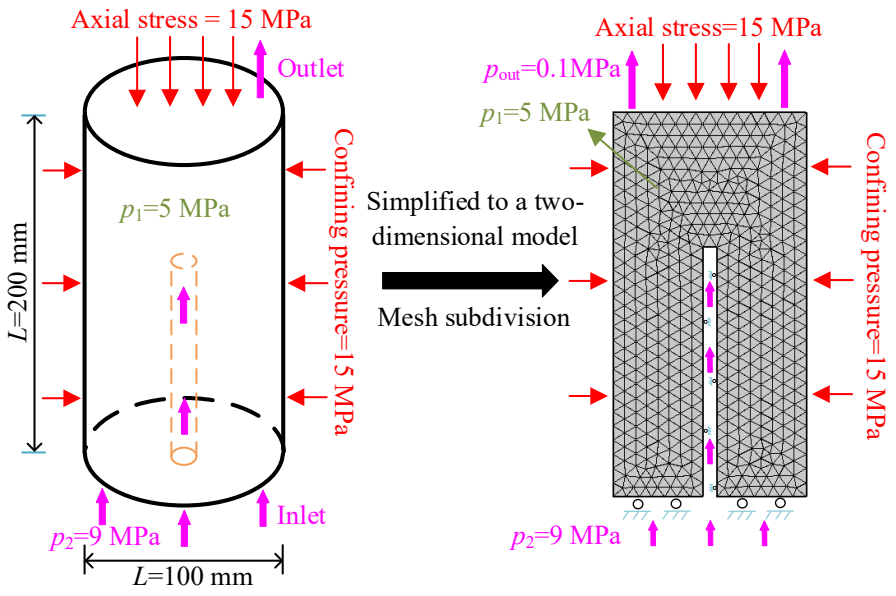

Fig.S2. Calculation model and definite solution condition of shale sample.

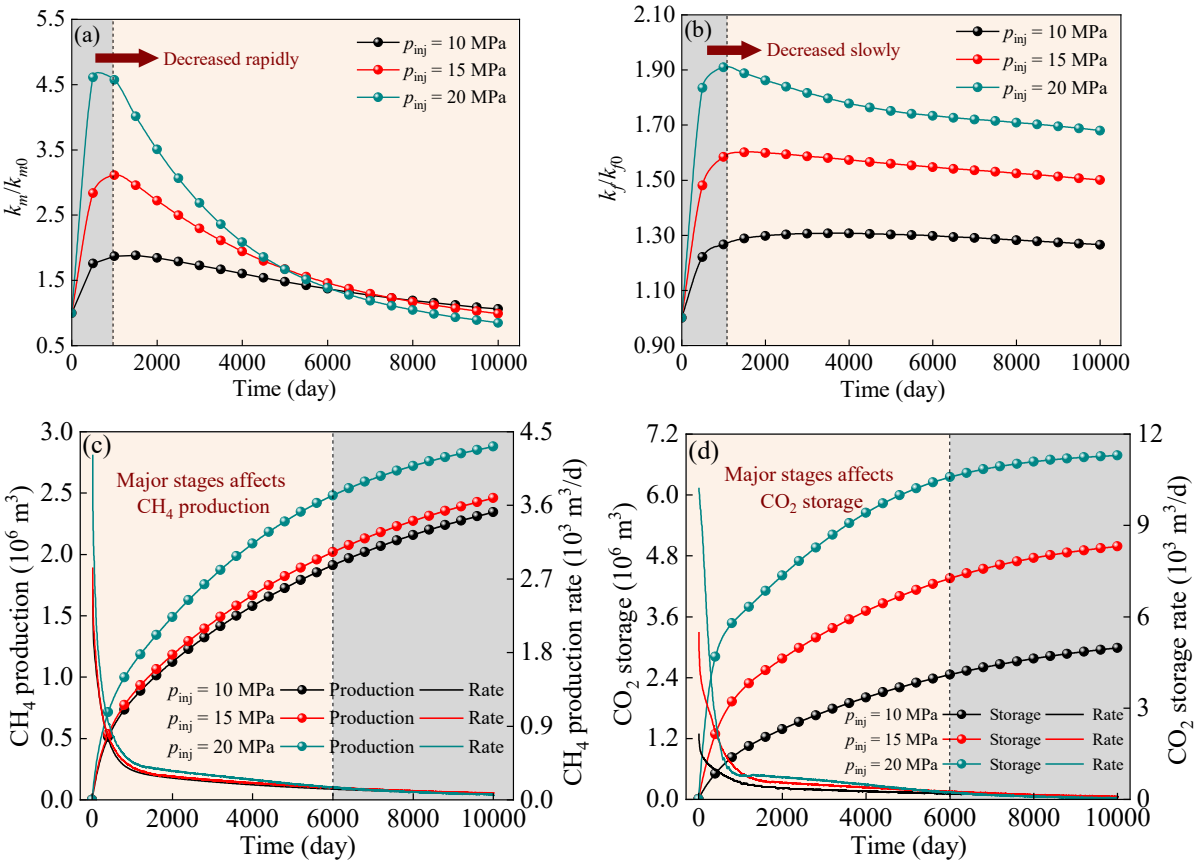

Fig.S3. Impact of injection pressure on the shale reservoir's (point D) (a) matrix, (b) fracture permeability, (c) CH_4 production, and (d) CO_2 storage.

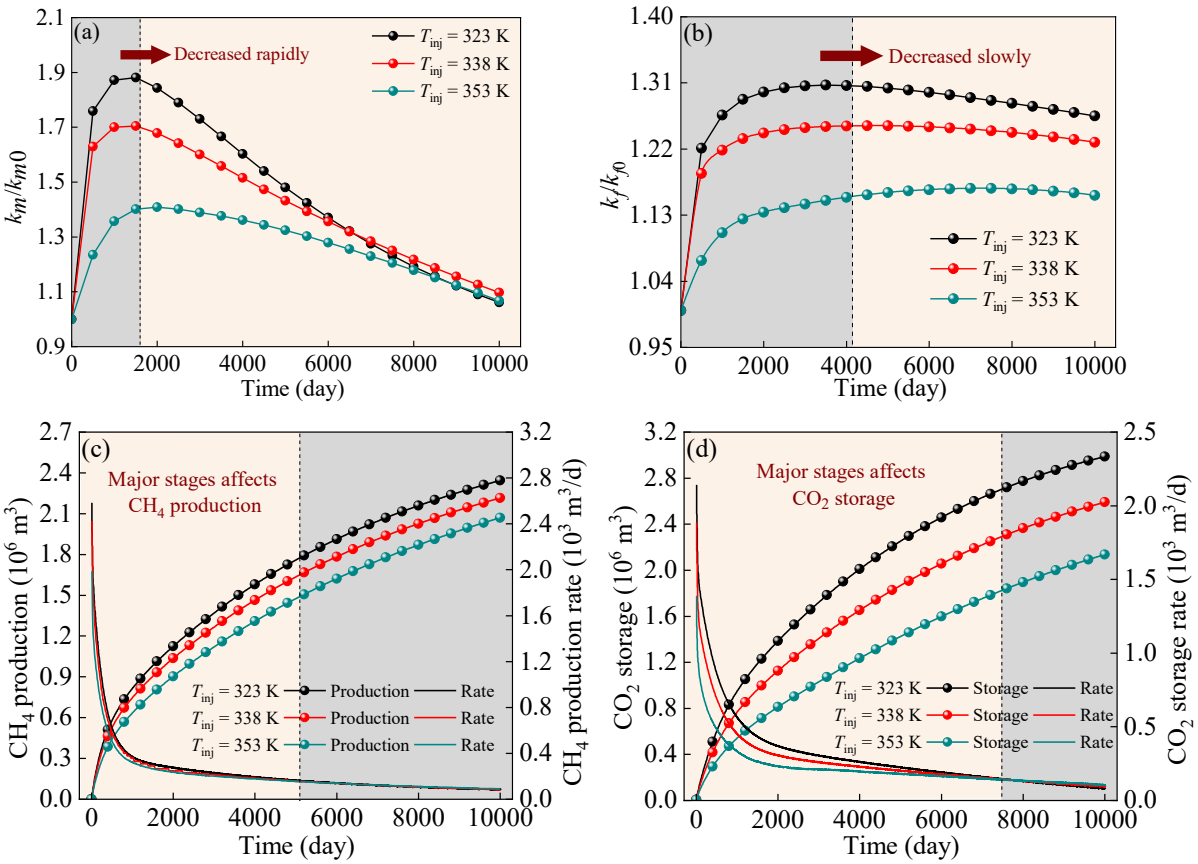

Fig.S4. Impact of injection temperature on the shale reservoir's (point D) (a) matrix and (b) fracture permeability, (c) CH_4 production, and (d) CO_2 storage.

Table S1 Key parameters used in model validation.

Parameter	Unit	Value	Parameter	Unit	Value
M_1, M_2	g/mol	16, 44	ρ_c	kg/m^3	2520
ϕ_{m0}	%	4.75	ρ_{s1}	kg/m^3	0.60
ϕ_{f0}	%	1.64	ρ_{s2}	kg/m^3	1.64
E	GPa	13.62	μ_1	Pa·s	1.26e-5
v	-	0.1147	μ_2	Pa·s	1.962e-5
K_f	GPa	4.28	Dv_1	m^2/s	2.11e-11
k_{f0}	mD	0.00435	Dv_2	m^2/s	2.32e-11
k_{m0}	mD	0.000367	K_{v1}	1/d	4.54
$\varepsilon_{L,1}$, $\varepsilon_{L,2}$	-	0.00054,0.00126	K_{v2}	1/d	2.99
$V_{L,1}$, $V_{L,2}$	m^3/kg	0.00210, 0.00695	λ_s	W/(m·K)	0.2
b_1, b_2	MPa^{-1}	0.309, 0.246	λ_{g1}	W/(m·K)	0.0409
C_c	J/(kg·K)	1380	λ_{g2}	W/(m·K)	0.0227
C_{g1}	J/(kg·K)	1809	α_T	K^{-1}	0.000024
C_{g2}	J/(kg·K)	792	r_0	nm	22.78

Table S2 Key numerical simulation parameters for CO_2-ESGR.

Parameter	Unit	Value	Parameter	Unit	Value
M_1, M_2	g/mol	16,44	C_{g2}	J/(kg·K)	844
ϕ_{m0}	%	5.54	ρ_c	kg/m^3	2470
ϕ_{f0}	%	0.66	ρ_{s1}	kg/m^3	0.60
E	GPa	61.3	ρ_{s2}	kg/m^3	1.64
v	-	0.217	μ_1	Pa·s	1.34e-5
K_f	GPa	10.0	μ_2	Pa·s	1.842e-5
k_{f0}	mD	0.0081	D_{v1}	m^2/s	3.66e-12
k_{m0}	mD	0.000217	D_{v2}	m^2/s	5.80e-12
$\varepsilon_{L,1}$, $\varepsilon_{L,2}$	-	0.00081,0.0036	K_v	1/s	5.24e-5
$V_{L,1}$, $V_{L,2}$	m^3/kg	0.00249,0.01009	λ_s	W/(m·K)	0.191
b_1, b_2	MPa^{-1}	0.311,0.099	λ_{g1}	W/(m·K)	0.0301
C_c	J/(kg·K)	1380	λ_{g2}	W/(m·K)	0.0137
C_{g1}	J/(kg·K)	2220	a_c, d_c, g_c	MPa^{-1}	2.27e-4, 0.0104, -0.0240
r_0	nm	22.78	b_c, e_c, h_c	K^{-1}	-2.98e-5, -0.0015, 0.0034
α_T	K^{-1}	0.000024	c_c, f_c, i_c	-	0.0493, 0.0809, -0.1623

Appendix B: CH_4 and CO_2 concentration distribution during conventional recovery and CO_2 enhanced recovery

A comparative analysis of CH_4 concentration distribution was conducted to evaluate the performance of conventional and CO_2-enhanced recovery methods. As shown in Fig. S5, the overall CH_4 concentration within the shale reservoir exhibits a decreasing trend over time, and the rate of CH_4 concentration decline is faster when utilizing CO_2 enhanced recovery methods. For conventional recovery without CO_2 injection, the CH_4 concentration near the production well in the shale reservoir decreases rapidly, while it increases with distance from the production well. After 250, 1,000, 5,000, and 10,000 days of production, the CH_4 concentration distribution within the shale reservoir ranges from 1,397 to 3,028 mol/m^3, 1,045 to 2,822 mol/m^3, 356 to 2,181 mol/m^3, and 156 to 1,678 mol/m^3, respectively. For CO_2 enhanced recovery, the CH_4 concentration within the shale reservoir at various time displays a pattern of low concentration near the wells, with higher concentrations in the intermediate section. After 250, 1,000, 5,000, and 10,000 days of production, the CH_4 concentration distribution within the shale reservoir ranges from 1,325 to 2,839 mol/m^3, 804 to 2,505 mol/m^3, 11.84 to 1,605 mol/m^3, and 7.01 to 1,053 mol/m^3, respectively.

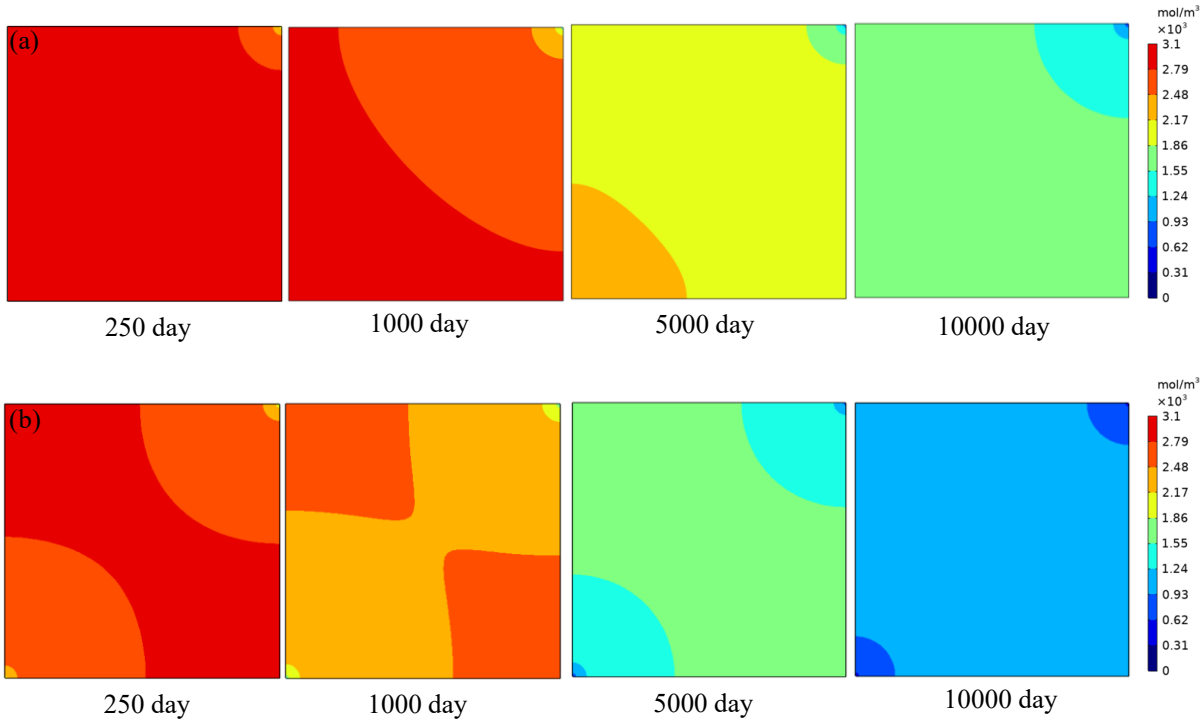

Fig.S5. CH_4 concentration distribution: (a) conventional recovery and (b) CO_2 enhanced recovery.

The CO_2 concentration distribution across the shale reservoir during CO_2 enhanced recovery is illustrated in Fig. S6. As CO_2 injection continues, the CO_2 concentration gradually increases as the gas migrates toward the production well. CO_2 exhibits a greater flow rate within the fractures compared to the matrix. After 250, 1,000, 5,000, and 10,000 days of production, the CO_2 stored within the fractures constitutes 97.21%, 80.10%, 56.20%, and 51.45% of the total CO_2 storage, respectively. The observation implies that the gas is

primarily distributed as a free phase within the shale fractures during the initial CO_2 injection period. With prolonged injection, CO_2 concentration increases gradually within the matrix, primarily in the adsorbed state (Kuang et al., 2024).

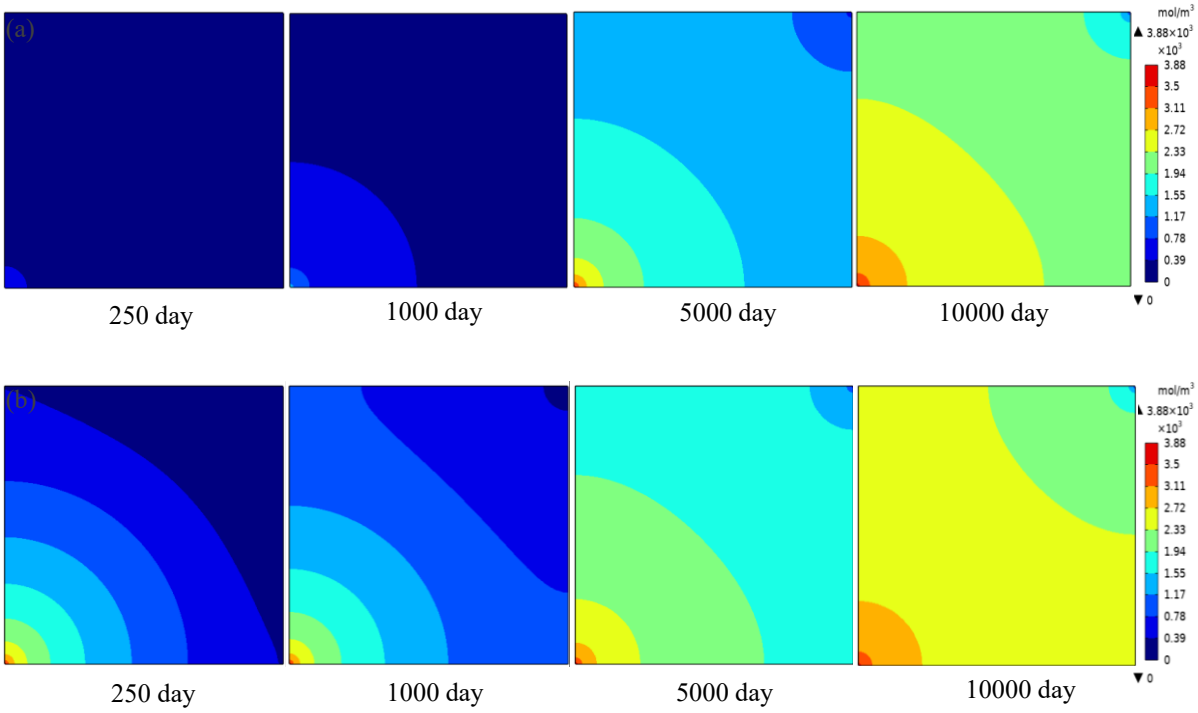

Fig.S6. CO_2 concentration distribution of shale during CO_2 enhanced recovery: (a) shale matrix and (b) fracture.

Appendix C: Impact of different influencing factors on gas concentration distribution

1. Reservoir stress

The distribution of gas within the shale reservoir is fundamentally controlled by reservoir stress conditions. Fig. S7 shows the impact of reservoir stress on the gas concentration within the shale reservoir (line AB). It can be found that the concentration curves of CH_4 consistently decline as time increases, while those of CO_2 steadily rise, and the change of the curve is more obvious during the initial period of CO_2 injection. Additionally, the overall CH_4 concentration curve rises as reservoir stress increasing, whereas the CO_2 concentration curve declines, which indicates that the increase of stress inhibits the flow of binary gas. Furthermore, it is observed that the impact of stress on CH_4 concentration varies with both spatial location and time. During the initial period of CO_2 injection, Stress has a limited impact on CH_4 and CO_2 concentration changes, primarily influencing CH_4 near the production well and CO_2 near the injection well. The location where stress affects CH_4 concentration gradually shifts from the production well towards the injection well as time increases, while the opposite trend is observed for CO_2.

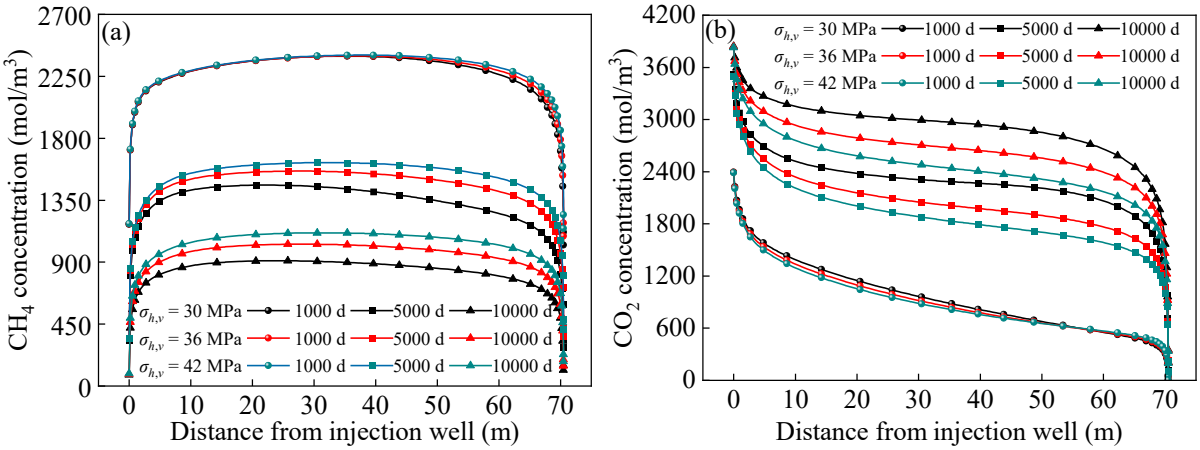

Fig.S7. Impact of reservoir stress on gas concentration in shale reservoir (Line AB): (a) CH_4 and (b) CO_2.

2. Injection pressure

The distribution of gas within the shale reservoir is fundamentally controlled by CO_2 injection pressure conditions during CO_2-ESGR. Fig. S8 shows the impact of CO_2 injection pressure on gas concentration within the shale reservoirs (line AB). It can be found that the CH_4 concentration curves significantly decline with elevated CO_2 injection pressure, while those of CO_2 significantly rises. This indicates that a high injection pressure enhances both CH_4 displacement and CO_2 injection. Compared to reservoir stress conditions, the CO_2 pressure has a more obvious impact on the CH_4 and CO_2 concentrations even during the initial injection period. It is observed that the coupling impacts of high-pressure differential and chemical dissolution enable injected CO_2 to migrate rapidly toward the production well under high injection pressure, thereby achieving efficient displacement.

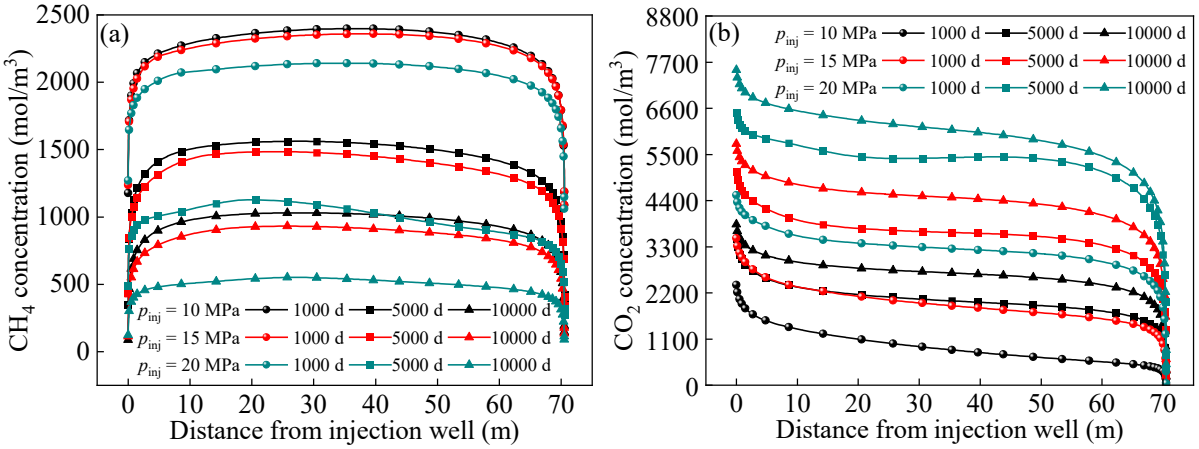

Fig.S8. Impact of injection pressure on gas concentration in shale reservoir (Line AB): (a) CH_4 and (b) CO_2.

3. Injection temperature

The distribution of gas within the shale reservoir is fundamentally controlled by CO_2 injection temperature conditions during CO_2-ESGR. Fig. S9 shows the impact of injection temperature on gas concentration within the shale reservoirs (line AB). It can be found that the CH_4 concentration curves significantly decline as the CO_2 injection temperature increases, while those of CO_2 significantly rises. However, there is an opposite trend in the position close to the injection well. This is primarily attributed to the higher temperature difference near the injection well after high-temperature CO_2 injection, resulting in stronger heat convection and conduction effects (Fan et al., 2019). The rapid rise in temperature causes rapid desorption of adsorbed CH_4 around the injection well, which in turn enhances the flow rate. Consequently, the CH_4 concentration decreases rapidly, while the CO_2 concentration increases rapidly near the injection well. In contrast, at locations farther from the injection well, the influence of thermal effects is relatively minor. Due to the stronger selective adsorption of CO_2 by shale under low-temperature conditions, the CH_4 concentration within the reservoir is lower under low injection temperatures at these distant locations.

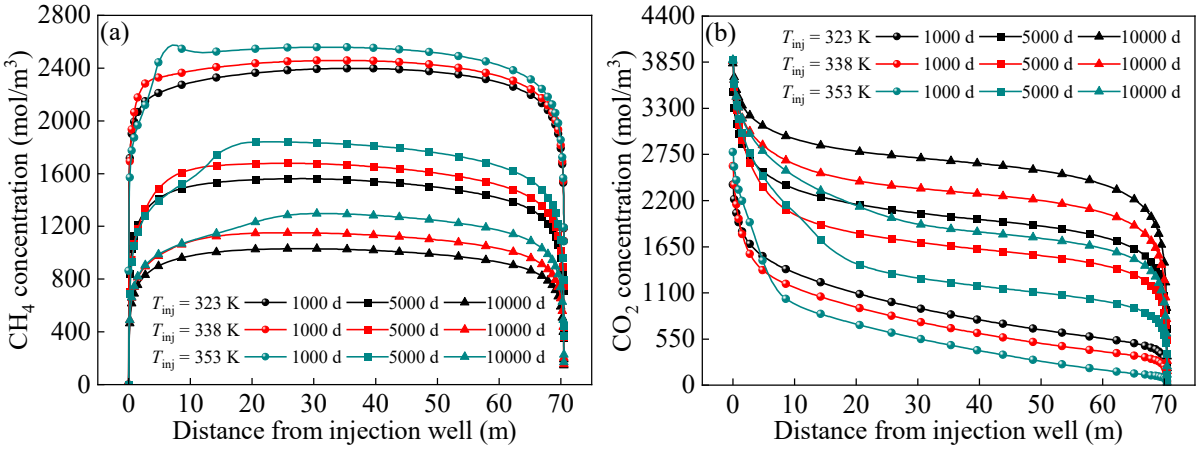

Fig.S9. Impact of injection temperature on gas concentration in shale reservoir (Line AB): (a) CH_4 and (b) CO_2.

4. Chemical dissolution-mechanical weakening (C-M) effect

The distribution of gas within the shale reservoir is controlled by chemical

dissolution-mechanical weakening effect during CO_2-ESGR. Fig. S10 shows the impact of C-M effect on gas concentration within the shale reservoirs (line AB). it can be found that the CH_4 concentration calculated without C-M effect is the highest, while the CH_4 concentration calculated without mechanical weakening effect (M effect) is the lowest. This is primarily attributed to chemical dissolution effect enlarging shale pore width, which promotes the flow of CH_4. Therefore, the CH_4 concentration calculated by the model incorporating the C-M effect and the model without incorporating the M effect is lower. On this basis, the mechanical weakening effect is further considered, the shale undergoes further compression under constant stress, leading to a mitigated trend of pore enlargement (Fatah et al., 2022; Yang et al., 2022), as a result, the CH_4 concentration increases. From Fig. S10 (b), it can be found that there is a corresponding relationship between the change of CO_2 concentration and the change of CH_4 concentration. The CO_2 concentration calculated without C-M effect is the lowest, while the CO_2 concentration calculated by the model incorporating C-M effect during the mid and late periods of CO_2 injection is the highest. The observed behavior is largely attributable to the influence of adsorption-induced swelling on shale permeability in this stage. Because the model considers the mechanical weakening effect, the shale pore fractures are further compressed under the same stress, which enhances shale's preferential adsorption of CO_2, resulting in higher CO_2 concentrations during the mid and late periods.

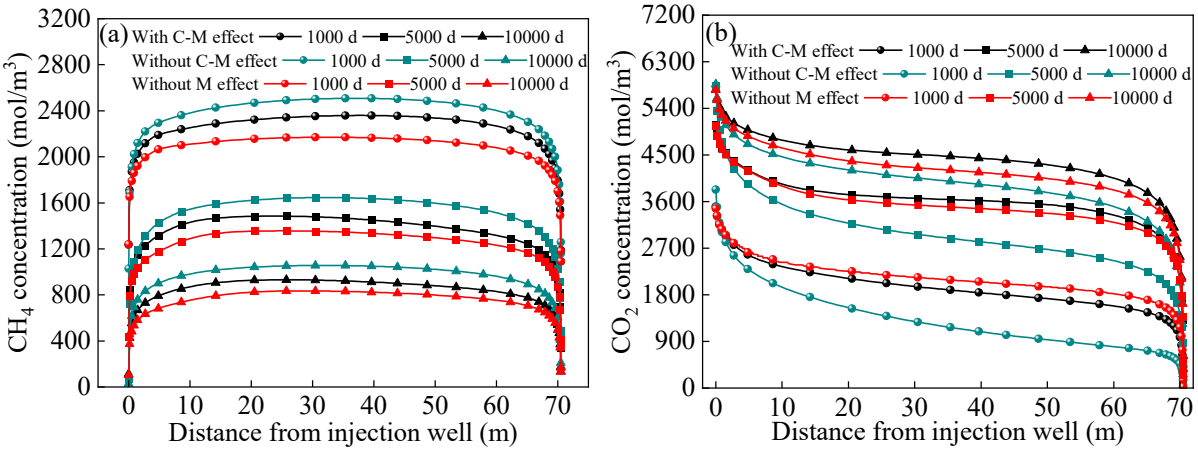

Fig.S10. Impact of chemical dissolution-mechanical weakening effect on gas concentration in shale reservoir (Line AB): (a) CH_4 and (b) CO_2.

References:

Fan, C., Elsworth, D., Li, S., et al. Thermo-hydro-mechanical-chemical couplings controlling CH_4 production and CO_2 sequestration in enhanced coalbed methane recovery. Energy, 2019, 173: 1054-1077.

Fatah, A., Mahmud, H., Bennour, Z., et al. Geochemical modelling of CO_2 interactions with shale: Kinetics of mineral dissolution and precipitation on geological time scales. Chemical Geology, 2022, 592: 120742.

Kuang, N., Zhou, J., Tian, S., et al. Fluid–solid coupling model with the multiple flow mechanism for CO_2-enhanced shale gas recovery and CO_2 sequestration. Energy & Fuels, 2024, 38(8): 7068-7084.

Yang, K., Zhou, J., Xian, X., et al. Chemical-mechanical coupling effects on the permeability of shale subjected to supercritical CO_2-water exposure. Energy, 2022, 248: 123591.